Multilayered $PdTe_2$/Thin Si Heterostructures as Self-powered Flexible Photodetectors with Heart Rate Monitoring Ability

Chengyun Dong, [1] *Xiang An,* [1] *Zhicheng Wu,* [1] *Zhiguo Zhu,* [1] *Chao Xie,* [2*] *Jian-An Huang,*[3] *and Linbao Luo*[1*]

[1] School of Microelectronics, Hefei University of Technology, Hefei, Anhui 230009, P. R. China

[2] Industry-Education-Research Institute of Advanced Materials and Technology for Integrated Circuits, Information Materials and Intelligent Sensing Laboratory of Anhui Province, Anhui University, Hefei, Anhui 230601, P. R. China

[3] Faculty of Medicine, Faculty of Biochemistry and Molecular Medicine, University of Oulu, 90220 Oulu, Finland

[*] Email: chaoxie@ahu.edu.cn, luolb@hfut.edu.cn

Abstract: Two-dimensional layered material/semiconductor heterostructures have emerged as a category of fascinating architectures for developing highly efficient and low-cost photodetection devices. Herein, we present the construction of a highly efficient flexible light detector operating in the visible-near infrared wavelength regime by integrating a $PdTe_2$ multilayer on a thin Si film. A representative device achieves a good photoresponse performance at zero bias including a sizeable current on/off ratio exceeding 10^4, a decent responsivity of ~343 mAW^{-1}, a respectable specific detectivity of ~2.56×10^{12} Jones, and a rapid response times of 4.5/379 μs, under 730 nm light irradiation. The detector also displays an outstanding long-term air stability and operational durability. In addition, thanks to the excellent flexibility, the device can retain its prominent photodetection performance at various bending radii of curvature and upon hundreds of bending tests. Furthermore, the large responsivity and rapid response speed endow the photodetector with the ability to accurately probe heart rate, suggesting the possibility for application in the area of flexible and wearable health monitoring.

Keywords: 2D layered material, heterostructure, flexible, photodetector, health monitoring

Introduction

Photodetectors are a group of photoelectric devices which covert photonic signals into electrical signals, and have found critical uses in vast kingdoms including light communication, optical imaging, security and environmental monitoring, medical diagnostics apparatus and so on.[1–4] Traditionally, commercial light detection devices are typically manufactured with inorganic semiconductor materials (*e.g.*, crystalline Si, Si/Ge heterostructures, group III-V semiconductors and alloys) and have gained excellent photoresponse features in the light wavelength spectrum of visible-near infrared (NIR) regimes.[2,5] However, further development

and vast applications of these devices are restricted by some existing dilemmas including epitaxially grown photoactive materials with good crystalline quality, complex device structures, intricate multistep fabricating procedures and expensive instruments requiring fine vacuum, *etc*. Over the last decades, there is an increasing interest in developing high-performance and low-cost photodetection devices by exploring novel functional materials such as quantum dots,[6,7] nanowires,[8–10] 2D layered materials,[11–14] hybrid perovskite materials,[15–17] and so on. As recently explored 2D layered materials, group-10 transition metal dichalcogenides (TMDs, *e.g.*, PtS_2, $PtSe_2$, $PdSe_2$, $PdTe_2$, *etc*.) have attracted extensive research attention in recent years because of their appealing physical characteristics including large charge carrier mobilities of over 1000 $cm^2V^{-1}s^{-1}$ in theory, layer-dependent adjustable bandgaps from 0-0.25 eV in bulk to 1.2-1.75 eV for single-layers, and prominent stability in ambient conditions.[12,18,19] Indeed, these prominent material features render group-10 TMDs very attractive for manufacturing broadband light detectors with photoresponse spanning from the visible to the NIR wavelength spectra.[20–23]

In order to further boost photoresponse performance of group-10 TMD-based photodetectors, an alternative approach is to explore hybrid heterostructures composed of 2D group-10 TMD/traditional three-dimensional (3D) semiconductor.[24–27] Compared with pure group-10 TMD-based device, the hybrid heterostructures can possibly offer following superiorities: (1) improved light absorption ability and widened optical absorption spectral regime due to additional light absorption from 3D semiconductor. (2) More effective separation and transport of photoexcited charge carriers thanks to existence of an internal electric field. (3) Self-powered photodetection ability at zero bias because of the strong photovoltaic effect. (4) Exotic functionalities brought by complementary features of both components. For instance, Yim *et al*. combined $PtSe_2$ multilayer with bulk Si to construct a wideband heterojunction light detector, which possesses a maximum responsivity of 490 mAW^{-1} and relatively poor responsivity of 0.1-1.5 mAW^{-1} at photon energies above and below the Si bandgap, respectively.[24] Wu and colleagues reported a self-powered broadband photodetector composed of a graphene/$PdSe_2$ multilayer/bulk Ge heterojunction.[25] Thanks to the anisotropic material properties of the $PdSe_2$, the light detector is highly polarization-sensitive with a record polarization sensitivity among 2D layered material-based photodetectors. Nevertheless, although significant achievements have been gained, the exploration of flexible photodetectors based on group-10 TMD/semiconductor heterostructures are thus far scarcely reported. On the other side, development of flexible and wearable health monitoring devices is becoming increasingly important nowadays due to deterioration of the environment and increasing diseases of people worldwide.[28,29]

In this work, by combing a $PdTe_2$ multilayer with a thin Si film, we report the construction of a flexible heterojunction photodetector, which can work in the visible-near infrared wavelength regions with outstanding photoresponse performance. At zero bias, the key performance figure-of-merits in terms of current on/off ratio, responsivity, specific detectivity and response speed can attain over 10^4, ~343 mAW^{-1}, ~2.56×10^{12} Jones, and 4.5/379 μs, respectively. In addition, the excellent photoresponse performance remains almost unchanged at different bending radii of curvature and upon hundreds of bending tests, suggesting eminent flexibility and operational durability of the device. What is more, it is also revealed that the light detector can accurately detect heart rate (HR) *via* photoplethysmography (PPG) test, which is highly desirable in real-time health monitoring application.

Results and discussion

Figure 1(a) depicts a diagrammatic sketch of the designed flexible photodetector composed of a $PdTe_2$ multilayer/thin Si heterostructure, and detailed fabricating procedures is provided in Figure S1. In brief, thin Si films with various thicknesses of about 10.5, 20.3, 30.2 and 40.3 μm were obtained by immersing pre-cleaned 500 μm-thick Si substrates in a KOH etchant for different etching durations of about 16, 14, 12 and 10 hours, respectively, at 100 °C in ambient conditions.[30] After etching, the thin Si film was washed with deionized water and transferred onto a flexible polyimide (PI) substrate. In-Ga alloy serving as Ohmic contact was daubed at the back side of the thin Si film. $PdTe_2$ multilayer was grown *via* a thermal-assisted tellurization technique using ~8 nm-thick Pd film as precursor and transferred onto the thin Si film to form a heterostructure with the help of a wet transfer technique.[31] Afterwards, a Ag electrode with a thickness of 80 nm was fabricated by using electron beam evaporation to form Ohmic contact with $PdTe_2$. Figure 2(b) displays the cross-sectional scanning electron microscopy (SEM) images of the fabricated thin Si films with diverse thicknesses, along with their optical images. It was seen that all thin Si films showed a very uniform thickness in a large area. In addition, all thin Si films can be readily bent, indicating a good flexibility. As expected, the flexibility increased with decreasing Si thickness. Considering that ~10.5 μm-thick Si film was prone to be broken, ~20.3 μm-thick Si film was employed for constructing flexible photodetectors in this work. The absorption spectrum of ~20.3 μm-thick Si film was tested and shown in Figure 1(c), demonstrating strong absorption of incident light spanning a broad wavelength spectrum in the range of the visible to NIR regions. Figure 1(d) plots the X-ray diffraction (XRD) pattern of the as-grown $PdTe_2$ multilayer, where notable diffraction peaks at 17.4°, 31.1°, 35°, 44°, 53° and 56° corresponded to (001), (011), (002), (110), (003) and (201) crystal planes of $PdTe_2$, respectively. No extra Pd or Te peaks were found, signifying high phase purity of the product. Indeed, as observed from the atomic force microscopy (AFM) image

(inset in Figure 1(e)), the $PdTe_2$ multilayer with a thickness of about 65 nm has a polycrystalline structure, which comprised vast dense crystalline domains having sizes ranging from about 100 to 360 nm.

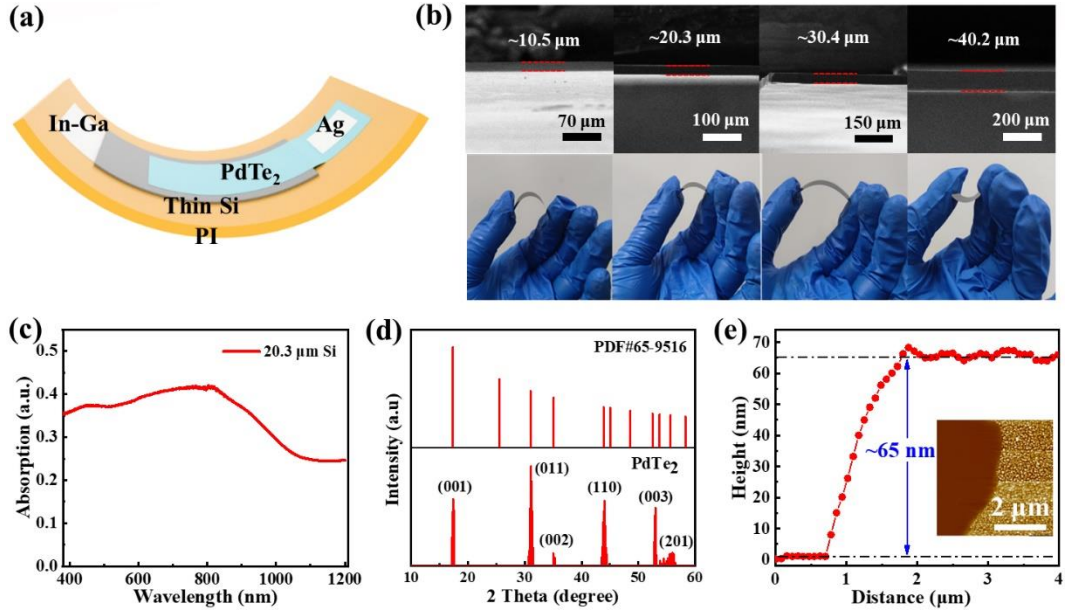

Figure 1. (a) Schematic diagram of the $PdTe_2$ multilayer/thin Si heterostructure-based flexible photodetector. (b) Cross-sectional SEM images (top panel) thin Si films with different thicknesses. The bottom panel shows photographs of thin Si films under bending conditions. (c) Absorption spectrum of a ~20.3 μm-thick thin Si film. (d) XRD pattern and (e) height profile of the multilayered $PdTe_2$ film. Inset in (e) displays an AFM image of the $PdTe_2$ multilayer.

Figure 2(a) displays the dark current-voltage (*I-V*) characteristic of a representative $PdTe_2$ multilayer/thin Si heterostructure, revealing a representative current rectifying feature. The forward-to-reverse ratio could approach 10^4 within the applied voltage of ±1 V, which was superior to $PtSe_2$ multilayer/Si (~100) and WS_2 multilayer/Si (~100) heterostructures in literatures.[24,32] Additionally, the ideality factor (n) of the heterostructure was calculated to be ~1.24, determined by the ln*I-V* characteristic shown in Figure S2(a).[33] Such a ideality factor closing to the value of an ideal diode (1) was superior to many similar heterostructures, including MoS_2 multilayer/Si (n=1.83) and $PtTe_2$ multilayer/Si (n=1.85).[34,35] Further, according to the theory of thermionic emission, the barrier height was calculated to be ~827 meV for this heterostructure (Figure S2(b)), which surpassed the values of heterostructures of few-layered $PtSe_2$/Si (~710 meV) and graphene/Si (~450 meV).[24,36] The above results signified the realization of a heterostructure with high-quality.

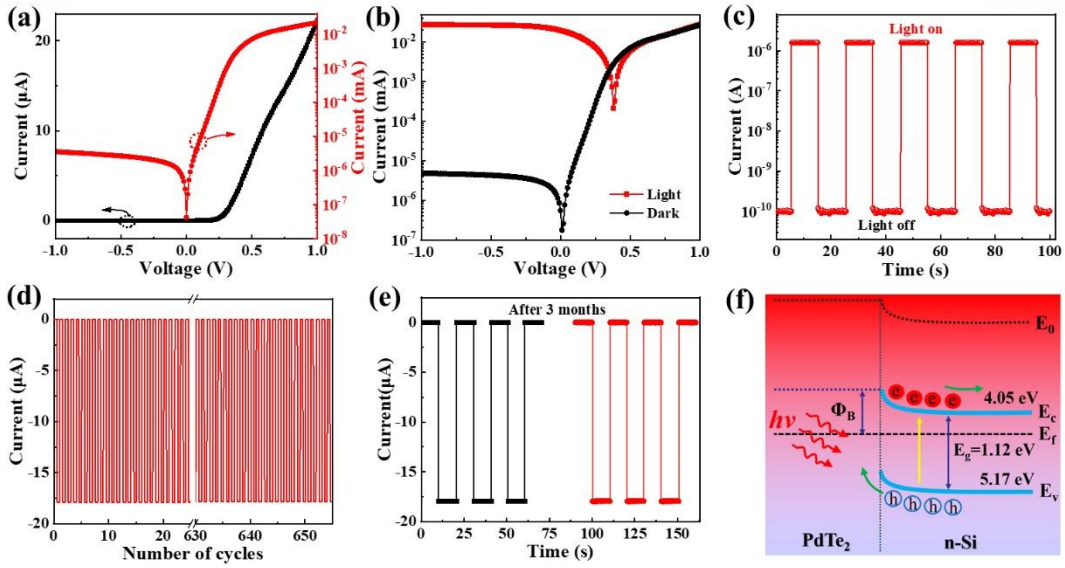

Figure 2. (a) Dark *I-V* curve of the $PdTe_2$ multilayer/thin Si heterostructure in linear and logarithmic coordinates. (b) The comparison of the *I-V* curves in darkness and upon 730 nm light irradiation. (c) Transient photoresponse upon periodically switched 730 nm light irradiation. Transient photoresponse (d) after over 650 cycles of working and (e) before and after 3 months' storage in air conditions. (f) Energy band diagram of the heterostructure upon light irradiation at 0 V.

The comparison of the *I-V* curves in darkness and upon light illumination was plotted in Figure 2(b). Clearly, under 730 nm light irradiation possessing an intensity of about 1.5 $mWcm^{-2}$, the heterostructure exhibited an obvious photovoltaic behavior with short circuit current and open circuit voltage of about 19.96 μA and 0.38 V, respectively. This feature enabled the heterostructure to function as a self-powered light detector operating at zero bias. The transient photoresponse upon periodically switched light illumination (~1.06 $mWcm^{-2}$) was further studied, as demonstrated in Figure 2(c). It was observed that the current could closely follow the rapid changing light signal, rendering repeatable and reversible high- and low-current statues with a sizeable current on/off ratio attaining about 1.5×10^4. It was also noted that the heterostructure device could quickly separate and collect the photogenerated charge carriers and held a rapid response speed as well, as evidenced by the sharp rise and fall edges in the transient photoresponse curve. Additionally, the present light detector possessed excellent operational stability and durability in ambient circumstances. Figure 2(d) and (e) display the transient photoresponse after over 650 cycles of operation and before and after 3 months' storage in air circumstances, respectively. One could see that both photocurrent and dark current maintained their initial values with negligible degradation. Therefore, the light detector could well maintain its prominent photo-switching characteristics.

Figure 2(f) illustrates the energy band diagram of the $PdTe_2$ multilayer/thin Si heterostructure, from which the physical mechanism of the above observed self-powered

photoresponse behavior could be understood. The work function values are ~4.80 eV and ~4.25 eV for the $PdTe_2$ multilayer featuring semi-metallic nature and the n-Si having a resistivity of 1-10 Ωcm^{-1}, respectively.[31] In case the two materials contacted with each other, the difference in work functions led to diffusion of electrons from n-Si to $PdTe_2$ up to attaining the thermal equilibrium state, which rendered the bending of the energy levels in the depletion region and formation of a internal electric field at heterostructure interface.[37] While the device was exposed to light irradiation holding photon energy higher than the bandgap of Si (1.12 eV), pairs of electrons and holes would be excited in the heterostructure. Those electrons and holes within or near the depletion region were rapidly separated by the strong internal electric field. Immediately, the electrons transferred across the thin Si film and gathered by bottom In-Ga contact, and the holes passed through the $PdTe_2$ and reached at Ag contact, giving production of sizeable photocurrent at zero bias.

We noted that such a self-powered photodetection characteristic relied strongly on the intensity of the incident light. Figure 3(a) displays the *I-V* curves in dark and under 730 nm light irradiation with diverse intensities for the device. Apparently, both the photovoltage and photocurrent at reverse and zero biases raised with increase in the light intensity. Specifically, the photocurrent at 0 V could raise from ~0.39 μA to as large as ~18.9 μA, as the change of the light intensity from about 7.84 μWcm^{-2} to 1.21 $mWcm^{-2}$. The transient photoresponse upon diverse light intensities was also explored and showed in Figure 3(b). It was observed that the transient photoresponse had the identical tendency as found in the *I-V* characteristics when changing the light intensity, and the light detector exhibited good photo-switching properties under various light illuminating conditions covering a wide intensity range. Generally, such a relationship between photocurrent and light intensity can be fitted by a extensively employed formula: : $I_{ph} \propto P^{\theta}$, where I_{ph} and P represent photocurrent and intensity of incident light, respectively, and θ denotes an empirical value relating to the activity of photocarrier recombination.[34] As displayed in Figure 3(c), fitting the curve of photocurrent at 0 V as a function of light intensity gave a large θ value of 0.8 approaching the ideal value of 1 at a low light intensity regime of 7.84 μWcm^{-2}-1.06 $mWcm^{-2}$ and a non-ideal value of 0.25 at a high light intensity region of 1.21-3.4 $mWcm^{-2}$, respectively. Thus, it could be inferred that the photocurrent loss owing to charge carrier recombination was weak at lower light intensity and became severe at higher light intensity.[33] The low light intensity region of 7.84 μWcm^{-2}-1.06 $mWcm^{-2}$ was within the linear dynamic range (LDR) of the light detector, and the photocurrent at 1.21 $mWcm^{-2}$ light intensity became deviation from the LDR of the device. Furthermore, by extrapolating to the dark current level (~10^{-10} A), the LDR of this device was deduced to be

about 104 dB, according to the formula: LDR=20log(I_{ph}^{*}/I_{dark}), where I_{ph}^{*} and I_{dark} represented the photocurrent deviating from linearity and dark current level, respectively.[38] This value was slightly lower than a commercial Si-based photodiode (120 dB) and could meet most application scenarios of photodetectors.[39]

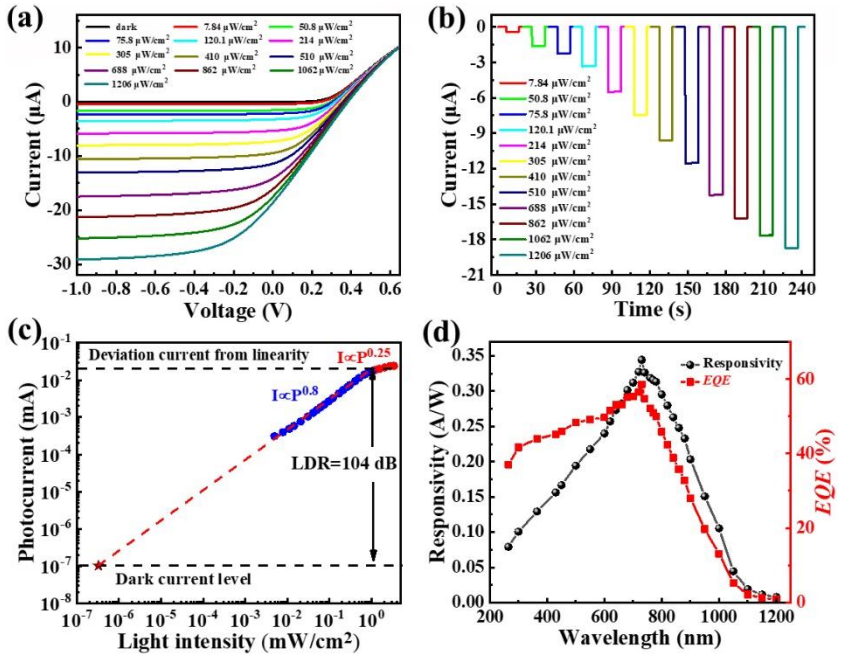

Figure 3. (a) *I-V* characteristics and (b) transient photoresponse of the heterostructure photodetector under 730 nm light irradiation with diverse intensities. (c) Photocurrent at 0 V *versus* intensity of incident light. The dark current level and deviation current from linearity determine the LDR of the light detector. (d) Dependence of responsivity and *EQE* on wavelength of incident light.

To facilitate the comparison of photoresponse performance of different light detectors, two pivotal performance figure-of-merits, *e.g.*, responsivity (*R*) and external quantum efficiency (*EQE*) were then studied based on the following equation:[11]

$$R = \frac{I_{ph}}{SP} = G(\frac{q\lambda}{hc})EQE \qquad (1)$$

where *S*, *G*, *q*, λ, *h* and *c* denote the effective device area (~0.09 cm^2), photocurrent gain, elementary charge, incident light wavelength, Planck's constant, and speed of light, respectively. The *G* can be considered as 1 in a normal photovoltaic-type detector absence of an internal gain mechanism.[37] Accordingly, the maximum *R* and *EQE* could attain approximately 343 mAW^{-1} and 58.6%, respectively, upon 730 nm light irradiation at zero bias. The sizeable *R* value was comparable to many light detectors comprising 2D layered material/Si heterostructures, including graphene/Si (435 mAW^{-1} at -2 V), MoS_2/Si (~300 mAW^{-1} at 0 V) and $PtSe_2$/Si (490 mAW^{-1} at 0 V).[24,34,36] In light of the relatively lower optical absorption because of reduced thickness in thin Si film, the *R* and *EQE* could be further enhanced by introducing anti-reflection

techniques such as employing light-trapping pyramid-Si structure.[40] The dependences of *R* and *EQE* on incident light wavelength were further investigated and displayed in Figure 3(d). We found that the present light detector held a sensitive photoresponse feature over a broad wavelength spectrum of 300-1000 nm with peak response at around 730 nm.

The ability of sensing weak light signals is critical for a photodetector, which is described by specific detectivity (D^*) as well as noise equivalent power (*NEP*). The two performance parameters are usually expressed as follows:[41]

$$D^* = \frac{(S\Delta f)^{1/2}}{NEP} \qquad (2)$$

$$NEP = \frac{\overline{i_n^2}^{1/2}}{R} \qquad (3)$$

where Δf and $\overline{i_n^2}^{1/2}$ represent the bandwidth and the root-mean-square value of the noise current, respectively. By doing Fourier transform of dark current recorded at zero bias, the $\overline{i_n^2}^{1/2}$ at the bandwidth of 1 Hz was estimated to be ~4.0×10^{-14} $AHz^{-1/2}$ (Figure S2(c) and (d)). Thus, the NEP was deduced to be ~1.17×10^{-13} $WHz^{-1/2}$, giving a respectable D^* of approximately 2.56×10^{12} Jones at zero bias.

We also examined the response speed of this device, which reflected its capability of detecting rapid varied optical signals. Figure 4(a) plots the transient photoresponse upon 730 nm light irradiation with different modulated frequencies. It was found that although the photoresponse experienced somewhat decline with increase in modulated frequency, the light detector could still exhibit a reversible and repeatable photoresponse with stable photo-switching characteristics even at a large frequency of 5000 Hz. From the curve of relative balance $(V_{max}-V_{min})/V_{max}$ *versus* modulated frequency (Figure 4(b)), the 3dB frequency described as the frequency where the photoresponse dropped to the 0.707 of the maximum photoresponse value was estimated to be about 1000 Hz.[42] In addition, as observed in Figure 4(c), the rise and fall times of response speed were determined to be 4.5 and 379 μs, respectively, which were comparable to many 2D layered material/Si heterostructure-based light detectors in literatures.[13,37]

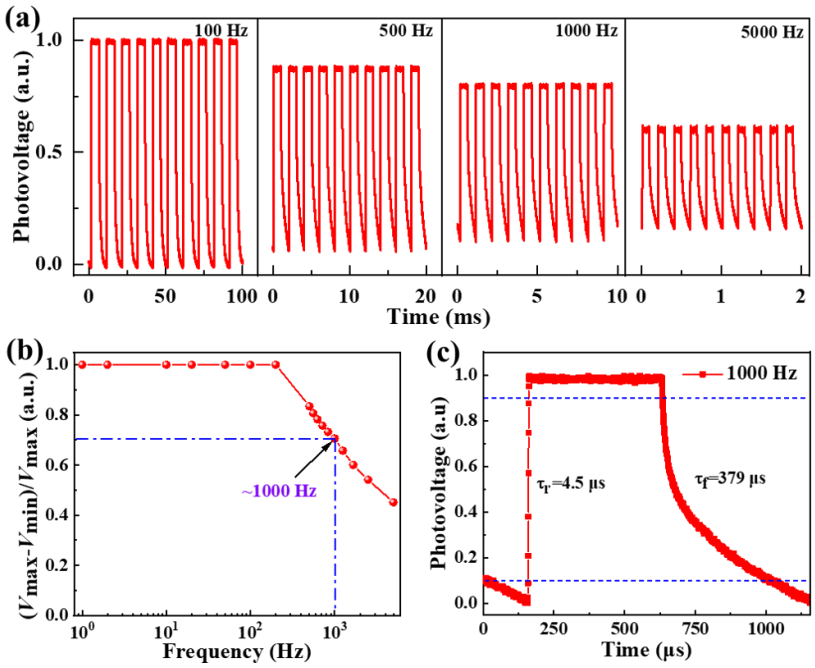

Figure 4. Transient photoresponse upon 730 nm light irradiation with various modulated frequencies. (b) Relative balance $(V_{max}\text{-}V_{min})/V_{max}$ *versus* incident light frequency, showing a 3dB frequency at about 1000 Hz. (c) An individual cycle transient photoresponse at 1000 Hz.

The excellent flexibilities of the ~20 μm-thick Si film and the $PdTe_2$ multilayer facilitated the present heterostructure to function as a flexible light detector. In this experiment, opposite sides of the PI substrate employed to fabricate the flexible device was fixed by using a vernier caliper, which could adjust the deformation degree of the substrate to attain various bending radii of curvature. Figure 5(a) plots the *I-V* characteristics in darkness and upon 730 nm light irradiation at different bending radii of curvature of ∞ (flat status), 0.65, 0.73, 0.85, 0.95 and 1.35 cm. The corresponding photocurrent and dark current derived from transient photoresponses were presented in Figure 5(b) as well. It was seen that despite some weak fluctuations in dark current, the photocurrent kept almost unchanged, suggesting that the present light detector could maintain its good photo-switching properties and operate well at different bending conditions. In addition, the photoresponse properties were also explored after hundreds of bending tests at a fixed bending radius of curvature of 0.85 cm. As displayed in Figure 5(c) and (d), the photocurrent showed negligible change, while the dark current even experienced somewhat decline after 100 and 200 cycles of bending tests, signifying robust stability of the light detector under repetitive mechanical bending. The fluctuation or decline in dark current might be caused by the slight variation in contact between thin Si film and In-Ga electrode when bending. Anyway, the above results unambiguously revealed the outstanding flexibility and operational durability of the $PdTe_2$ multilayer/thin Si heterostructure-based flexible photodetector.

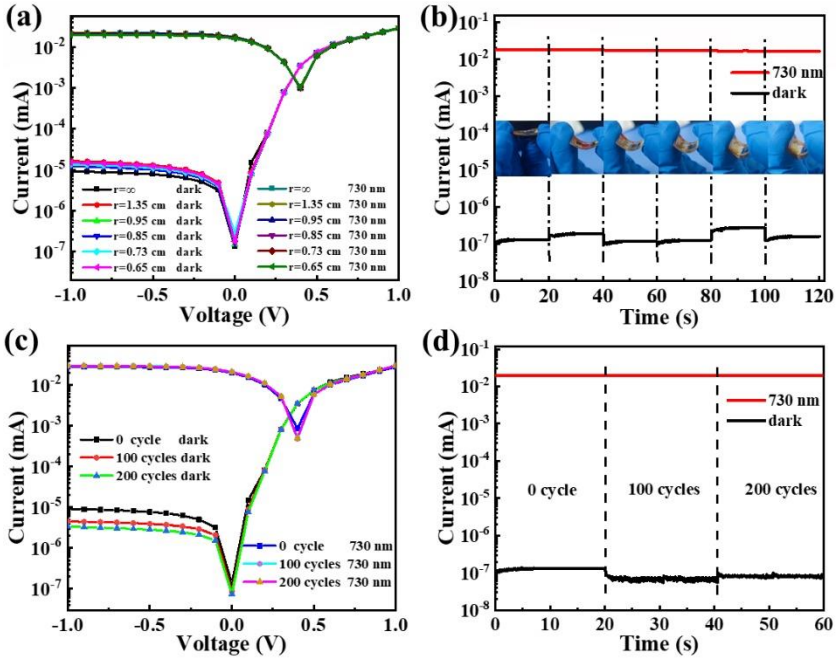

Figure 5. (a) *I-V* curves and (b) dark current and photocurrent of the heterostructure-based flexible light detector under different bending radii of curvature. (c) *I-V* curves and (d) photocurrent and dark current of the heterostructure-based flexible light detector before and after 100 and 200 cycles of bending tests.

The collective features of the present heterostructure-based light detector, *e.g.*, the sizeable photoresponse spanning the absorption spectrum of hemoglobin as well as the short response times, afforded it with the ability to serve as a photoplethysmography (PPG) sensor for HR detection.[43,44] Figure 6(a) and (b) demonstrate the schematic diagram and experimental setup for HR detection using this device, respectively. A 730 nm light beam transmitted through finger tissue of a volunteer and reached the underlying light detector. During cardiac cycles, the alteration of blood-volume in the veins was converted to pulsatile signals collected by a SourceMeter, from which the HR data could be extracted. Figure 6(c) and (d) present the obtained pulse PPG signals of the volunteer at normal and immediately after exercise statuses, respectively. The HR at the two conditions was deduced to be 70.8 and 118.8 beats/min, respectively, *via* dividing 60 s using the average interbeat interval of both cases. It was found that the obtained HR values at both conditions were well coincident with the recording values of a commercial Mi smart bracelet (71 and 118 beats/min, see insets in Figure 6(c) and (d)), suggesting high accuracy of heterostructure device for HR detection. In consideration of its good flexibility, the present light detector might hold huge prospect for use in flexible and even wearable health monitoring devices.

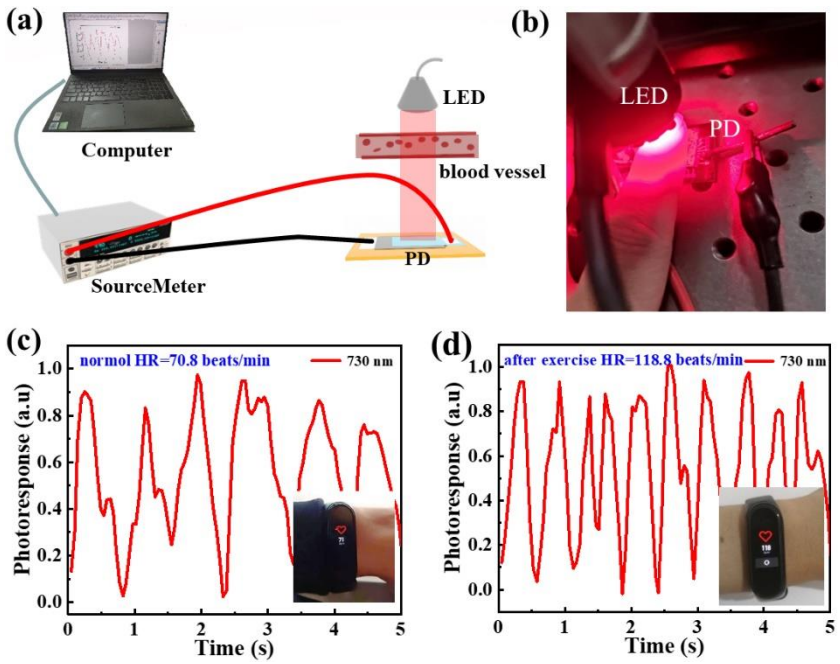

Figure 6. (a) Schematic diagram and (b) experimental setup of the HR detection system. LED and PD represent light emitting diode and photodetector, respectively. Normalized transient photoresponse of the heterostructure (c) at normal and (d) after exercise conditions (upon 730 nm light illumination). Insets in (c) and (d) are photographs of a commercial Mi smart bracelet, showing HR measurement results at normal and after exercise statuses, respectively.

Conclusions

In conclusion, we have demonstrated the construction of a highly efficient self-powered flexible photodetector by combing a $PdTe_2$ multilayer with a thin Si film. The as-fabricated heterostructure exhibited a wideband photoresponse covering the wavelength spectrum of the visible-NIR regions with current on/off ratio, responsivity, specific detectivity and response speed attaining 10^4, ~343 mAW^{-1}, 2.56×10^{12} Jones and 4.5/379 μs, respectively, upon 730 nm light irradiation at zero bias. In addition, the heterostructure light detector possessed excellent flexibility, robust operational durability and long-term air stability. The outstanding photoresponse characteristics also endowed the device with good HR detection functionality. The present flexible light detector might find important applications in flexible and even wearable health monitoring devices.

Acknowledgements

This work was financially supported by the National Natural Science Foundation of China (NSFC, Nos. 62275002, 51902078, 62074048, 62075053), the Anhui Provincial Natural Science Foundation (2008085MF205), and the Fundamental Research Funds for the Central Universities (JZ2020HGTB0051, PA2020GDKC0024).

References

1 F. H. L. Koppens, T. Mueller, P. Avouris, A. C. Ferrari, M. S. Vitiello and M. Polini, *Nat. Nanotechnol.*, 2014, **9**, 780–793.

2 M. Buscema, J. O. Island, D. J. Groenendijk, S. I. Blanter, G. A. Steele, H. S. J. van der Zant and A. Castellanos-Gomez, *Chem. Soc. Rev.*, 2015, **44**, 3691–3718.

3 M. Long, P. Wang, H. Fang and W. Hu, *Adv. Funct. Mater.*, 2019, **29**, 1803807.

4 H. Fang and W. Hu, *Adv. Sci.*, 2017, **4**, 1700323.

5 C. Xie and F. Yan, *Small*, 2017, **13**, 1701822.

6 A. Ren, L. Yuan, H. Xu, J. Wu and Z. Wang, *J. Mater. Chem. C*, 2019, **7**, 14441–14453.

7 J. Wu, Y. Lu, S. Feng, Z. Wu, S. Lin, Z. Hao, T. Yao, X. Li, H. Zhu and S. Lin, *Adv. Funct. Mater.*, 2018, **28**, 1804712.

8 T. Zhai, L. Li, Y. Ma, M. Liao, X. Wang, X. Fang, J. Yao, Y. Bando and D. Golberg, *Chem. Soc. Rev.*, 2011, **40**, 2986–3004.

9 T. Zhai, X. Fang, L. Li, Y. Bando and D. Golberg, *Nanoscale*, 2010, **2**, 168.

10 J. Jie, W. Zhang, I. Bello, C. S. Lee and S. T. Lee, *Nano Today*, 2010, 5, 313–336.

11 C. Xie, C. Mak, X. Tao and F. Yan, *Adv. Funct. Mater.*, 2017, **27**, 1603886.

12 L. Pi, L. Li, K. Liu, Q. Zhang, H. Li and T. Zhai, *Adv. Funct. Mater.*, 2019, **29**, 1904932.

13 C. Liu, J. Guo, L. Yu, J. Li, M. Zhang, H. Li, Y. Shi and D. Dai, *Light Sci. Appl.*, 2021, **10**, 123.

14 J. Yao and G. Yang, *Nanoscale*, 2020, **12**, 454–476.

15 W. Tian, H. Zhou and L. Li, *Small*, 2017, **13**, 1702107.

16 H. Wang and D. H. Kim, *Chem. Soc. Rev.*, 2017, **46**, 5204–5236.

17 C. Xie, C. Liu, H. Loi and F. Yan, *Adv. Funct. Mater.*, 2020, **30**, 1903907.

18 Z. Yan, H. Yang, Z. Yang, C. Ji, G. Zhang, Y. Tu, G. Du, S. Cai and S. Lin, *Small*, 2022, **18**, 2200016.

19 Y. Zhao, J. Qiao, Z. Yu, P. Yu, K. Xu, S. P. Lau, W. Zhou, Z. Liu, X. Wang, W. Ji and Y. Chai, *Adv. Mater.*, 2017, **29**, 1604230.

20 X. Yu, P. Yu, D. Wu, B. Singh, Q. Zeng, H. Lin, W. Zhou, J. Lin, K. Suenaga, Z. Liu and Q. J. Wang, *Nat. Commun.*, 2018, **9**, 1545.

21 L. Li, W. Wang, Y. Chai, H. Li, M. Tian and T. Zhai, *Adv. Funct. Mater.*, 2017, **27**, 1701011.

22 Q. Liang, Q. Wang, Q. Zhang, J. Wei, S. X. Lim, R. Zhu, J. Hu, W. Wei, C. Lee, C. Sow, W. Zhang and A. T. S. Wee, *Adv. Mater.*, 2019, 1807609.

23 C. Guo, Y. Hu, G. Chen, D. Wei, L. Zhang, Z. Chen, W. Guo, H. Xu, C.-N. Kuo, C. S. Lue, X. Bo, X. Wan, L. Wang, A. Politano, X. Chen and W. Lu, *Sci. Adv.*, 2020, **6**, eabb6500.

24 C. Yim, N. McEvoy, S. Riazimehr, D. S. Schneider, F. Gity, S. Monaghan, P. K. Hurley, M. C. Lemme and G. S. Duesberg, *Nano Lett.*, 2018, **18**, 1794–1800.

25 D. Wu, J. Guo, J. Du, C. Xia, L. Zeng, Y. Tian, Z. Shi, Y. Tian, X. J. Li, Y. H. Tsang and J. Jie, *ACS Nano*, 2019, **13**, 9907–9917.

26 L.-H. Zeng, D. Wu, S.-H. Lin, C. Xie, H.-Y. Yuan, W. Lu, S. P. Lau, Y. Chai, L.-B. Luo, Z.-J. Li and Y. H. Tsang, *Adv. Funct. Mater.*, 2019, **29**, 1806878.

27 L. Luo, D. Wang, C. Xie, J. Hu, X. Zhao and F. Liang, *Adv. Funct. Mater.*, 2019, **29**, 1900849.

28 C. Chen, K. Li, F. Li, B. Wu, P. Jiang, H. Wu, S. Lu, G. Tu, Z. Liu and J. Tang, *ACS Photonics*, 2020, **7**, 352–360.

29 Y. Xu, H. Shen, Y. Li, Z. Yue, W. Zhang, Q. Zhao and Z. Wang, *ACS Appl. Electron. Mater.*, 2022, **4**, 4641–4652.

30 K. Ruan, K. Ding, Y. Wang, S. Diao, Z. Shao, X. Zhang and J. Jie, *J. Mater. Chem. A*, 2015, **3**, 14370–

14377.
31 Y. Liang, C. Xie, C. Dong, X. Tong, W. Yang, C. Wu and L. Luo, *J. Mater. Chem. C*, 2021, **9**, 14897–14907.
32 E. Wu, D. Wu, C. Jia, Y. Wang, H. Yuan, L. Zeng, T. Xu, Z. Shi, Y. Tian and X. Li, *ACS Photonics*, 2019, **6**, 565–572.
33 X. Li, M. Zhu, M. Du, Z. Lv, L. Zhang, Y. Li, Y. Yang, T. Yang, X. Li, K. Wang, H. Zhu and Y. Fang, *Small*, 2016, **12**, 595–601.
34 L. Wang, J. Jie, Z. Shao, Q. Zhang, X. Zhang, Y. Wang, Z. Sun and S.-T. Lee, *Adv. Funct. Mater.*, 2015, **25**, 2910–2919.
35 L. Zeng, D. Wu, J. Jie, X. Ren, X. Hu, S. P. Lau, Y. Chai and Y. H. Tsang, *Adv. Mater.*, 2020, **32**, 2004412.
36 X. An, F. Liu, Y. J. Jung and S. Kar, *Nano Lett.*, 2013, **13**, 909–916.
37 C. Xie, Y. Wang, Z. X. Zhang, D. Wang and L. B. Luo, *Nano Today*, 2018, **19**, 41–83.
38 F. P. García de Arquer, A. Armin, P. Meredith and E. H. Sargent, *Nat. Rev. Mater.*, 2017, **2**, 16100.
39 X. Gong, M. Tong, Y. Xia, W. Cai, J. S. Moon, Y. Cao, G. Yu, C.-L. Shieh, B. Nilsson and A. J. Heeger, *Science*, 2009, **325**, 1665–1667.
40 P. Xiao, J. Mao, K. Ding, W. Luo, W. Hu, X. Zhang, X. Zhang and J. Jie, *Adv. Mater.*, 2018, **30**, 1801729.
41 J. Li, L. Niu, Z. Zheng and F. Yan, *Adv. Mater.*, 2014, **26**, 5239–5273.
42 J. D. Yao, Z. Q. Zheng and G. W. Yang, *Prog. Mater. Sci.*, 2019, **106**, 100573.
43 C. M. Lochner, Y. Khan, A. Pierre and A. C. Arias, *Nat. Commun.*, 2014, **5**, 5745.
44 H. Xu, J. Liu, J. Zhang, G. Zhou, N. Luo and N. Zhao, *Adv. Mater.*, 2017, **29**, 1700975.